1999

Magnetic circuit of a synchronous reluctance motor

P P. Ciufo
University of Wollongong, ciufo@uow.edu.au

D. Platt
University of Wollongong, dplatt@uow.edu.au

B S. P Perera
University of Wollongong

Publication Details

P. P. Ciufo, D. Platt & B. S. P. Perera, "Magnetic circuit of a synchronous reluctance motor," Electric Machines and Power Systems, vol. 27, (3) pp. 253-270, 1999.

Magnetic circuit of a synchronous reluctance motor

Abstract
This paper presents a model of the magnetic circuit for an axially laminated synchronous reluctance motor. The basis of the modelling technique is the determination of a value for an equivalent ``q-channel'' reluctance. This reluctance contains all the effects of paths available to q-axis flux through the rotor body. Expressions for the distribution of airgap and other motor fluxes have been developed from basic analyses involving mmf and continuity of flux. The foundations of all of these expressions are the physical parameters of the motor. The equations developed have been applied to a 370 W motor and the results from models presented are compared with results obtained from a finite element analysis of the same motor where good agreement has been achieved.

Keywords
motor, circuit, magnetic, synchronous, reluctance

Disciplines
Engineering | Science and Technology Studies

Publication Details
P. P. Ciufo, D. Platt & B. S. P. Perera, "Magnetic circuit of a synchronous reluctance motor," Electric Machines and Power Systems, vol. 27, (3) pp. 253-270, 1999.

MAGNETIC CIRCUIT OF A SYNCHRONOUS RELUCTANCE MOTOR

P. P. CIUFO, D. PLATT and B. S. P. PERERA
Department of Electrical and Computer Engineering
University of Wollongong,
Wollongong, NSW 2522, Australia.

ABSTRACT

This paper presents a model of the magnetic circuit for an axially laminated synchronous reluctance motor. The basis of the modelling technique is the determination of a value for an equivalent "q-channel" reluctance. This reluctance contains all the effects of paths available to q-axis flux through the rotor body. Expressions for the distribution of airgap and other motor fluxes have been developed from basic analyses involving mmf and continuity of flux. The foundations of all of these expressions are the physical parameters of the motor. The equations developed have been applied to a 370 W motor and the results from models presented are compared with results obtained from a finite element analysis of the same motor where good agreement has been achieved.

1 INTRODUCTION

In the field of A.C. motor research, there continues to be a steady increase in activity associated with the modelling of the Synchronous Reluctance Motor (SRM). Much of this modelling involves determination of torque and motor fluxes using the physical parameters of the motor such as slot width and depth [1–5]. Other modelling attempts have been made utilising motor parameters such as d-axis inductance and q-axis inductance, but without referring to the process of determining such quantities [6,7]. A third level of modelling has been the optimisation of rotor design to produce better or more predictable torque characteristics [8–11]. Perhaps the last level of activity is in the design of the stator windings to improve motor performance or control [12]. These levels of modelling are important since they provide an insight into the dependencies of the motor characteristics on the physical design of the motor.

For any particular motor with a given rotor position, it is possible to construct a magnetic circuit which describes it with a reasonable degree of accuracy. We would simply assume that all the sections of iron were magnetic short circuits (nodes) and that the airgaps separating these pieces of iron could be represented by linear reluctances which can be calculated by well known formulae. This circuit would then behave like a linear resistive electrical network and its solution would be straightforward. The resistive network would be a combination of series and parallel circuits, each representing a particular reluctance or permeance [3]. Such an approach should produce results which are very similar to those obtained by finite element methods but significantly faster in terms of computation time. This approach should also produce an analytical model with similar accuracy, but easier to manipulate, which gives deeper insight into the nature of the motor.
The process of identifying the correct relationships between the iron and the airgaps is one that needs careful consideration. The analysis of the SRM in this paper hinges on the concept of zigzag flux paths. We propose that there exists a flux path for the q-axis flux that allows multiple crossings of the airgap into the stator.
This flux path and the non-zigzag path can be characterised by an equivalent q-channel reluctance. The q-axis channel reluctance is defined as the average reluctance associated with the q-axis flux path where the rotor body is present. The expression for this value can be determined using the idea of modelling the circuit as a network of parallel and series circuits. The approach used in this paper produces a model that allows the prediction of total flux, for example, of the motor.

2 THE Q-AXIS RELUCTANCE CHANNEL MAGNETIC CIRCUIT

The type of motor under consideration is a SRM with an anisotropic rotor that is axially laminated. The rotor laminations, both magnetic and non-magnetic, are relatively thin and should be of the order of 10% of the thickness of a stator lamination tooth stem in order to observe the effects described in this paper. Such a rotor is illustrated in Figure 1. Note that this figure is purely a conceptual illustration and not a detailed design.

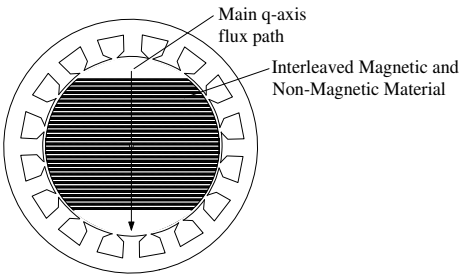

Figure 1: Anisotropic Rotor

Consider the way that flux passes in the direction of the q-axis in a section of the rotor body well away from the pole edges, toward the centre of the rotor. There is the main flux path directly through the body of the rotor, passing through the magnetic and non-magnetic laminations of the rotor. There is also a flux path available that allows the q-axis flux to move in a zigzag fashion and cross the rotor-stator airgap many times. If a “snapshot” is taken of the rotor at any instant in time, sections of the rotor laminations can be identified

which pass flux from a stator tooth on one side of the rotor to a stator tooth on the other side. This section will represent negligible reluctance between these teeth, through the rotor body, but there will still be the reluctance of the airgaps. The adjacent section of laminations in the rotor align between a stator tooth on one side of the stator and a slot opening on the other. Accordingly, these laminations are unable to pass zigzag flux between teeth on opposite sides of the stator. However, it is still capable of passing flux across the body of the rotor and is therefore represented as a simple reluctance in that direction.

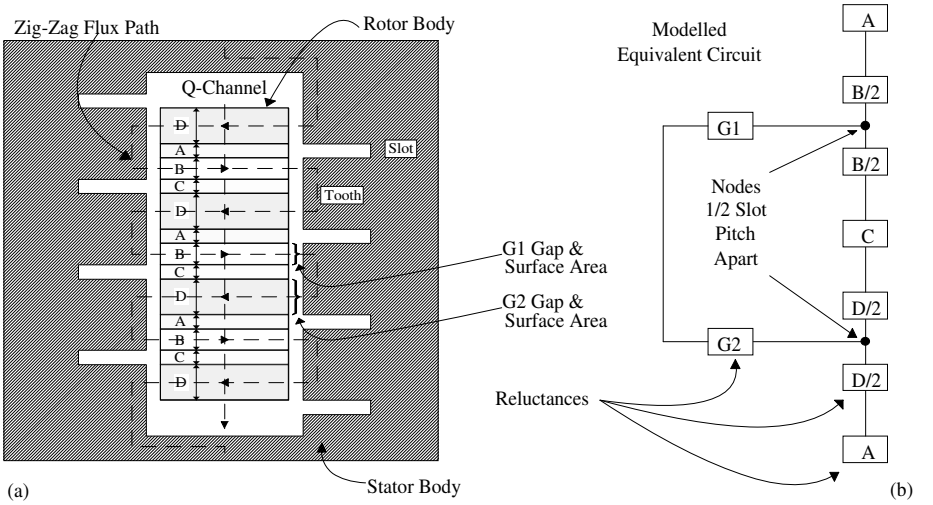

Figure 2: (a)Q-Axis Reluctance Model, (b)Equivalent Circuit

The diagram of Figure 2 is best described as that of a developed section from a reluctance motor. The diagonally striped area represents the stator body. The zigzag flux will find its way through the rotor and stator body as shown. The rotor body of Figure 2(a) is classified into sections labelled A to D. These sections do not represent the alternate magnetic and non-magnetic laminations found in an axially laminated rotor. Instead, they represent sections through the rotor body that either facilitate or prevent the passing of zigzag flux from one side of the stator to the other. Each section would consist of both magnetic and non-magnetic laminations.

Section D is located between a tooth on one side of the stator and a tooth on the other side. The zigzag flux is expected to traverse this path since it represents a path of low reluctance from one side of the stator to the other. Section A is different to section D since it represents the area opposite a slot opening. The zigzag flux is assumed not go across this section (from left to right or vice versa) as the slot opening is a high reluctance path. The next section, section B, is similar to section D, except the thickness of this area is smaller compared to section D. Likewise, section C is similar to section A.

The thickness of these sections depends on the alignment between the rotor and stator. As the rotor spins, the alignment of the slot openings on either side of Figure 2(a) will change. Since the modelling technique that is proposed here does not seek to define exact values of reluctance but rather quantities that are useful for an analytical model of the motor, average reluctance is the quantity required. The two extremes of alignment have the stator slots exactly aligned for the case of maximum reluctance greater than the average value and the

slots exactly misaligned for the case of minimum reluctance less than the average value. The alignment in Figure 2(a) should be interpreted as that alignment which models the average reluctance of the q-channel. This case represents an alignment half way between the two extremes.
The whole rotor body is made up of sections which may be represented in one of these four ways (A, B, C or D). Thus, we may draw a magnetic circuit which represents the path of the q-axis flux through the rotor. Such a circuit is illustrated in Figure 2(b).
The three series reluctances, located in parallel between the $\frac{1}{2}$ slot pitch nodes of Figure 2(b), represent reluctances through the body of rotor. Included is the reluctance that represents the airgap at either end of the q-axis main flux path. This is generally a significant reluctance that can be complicated by the shape of the rotor surface. In the modelling presented in this paper, a constant value for reluctance in this airgap is used. Appendix B gives the mathematical expressions for all of the reluctances discussed in this section.

3 FINITE ELEMENT ANALYSIS

Evidence for the existence of the zigzag effect can be found through the use of Finite Element (FE) analysis. Indeed, such an analysis is vital in the measurement of these effects since practical results are virtually impossible to obtain. The SRM that is the subject of the study in this paper has also been modelled using FE tools. Whilst this paper is not intended to produce detailed results of this simulation, some outcomes from the work provide good correlation and support for the analytical modelling.
Evidence of the zigzag flux can be clearly seen on some of the results of the FE simulations. By modelling the SRM with thin rotor laminations and using a current intended to produce q-axis flux, misalignment of the rotor by $\frac{1}{4}$ of a slot pitch will introduce the zigzag effect. Such a misalignment forms flux paths that connect the stator teeth from one side of the rotor to the opposite side. If the rotor laminations are too thick, then this effect was found to be absent or found to be unobservable. The finite element model used for this work has a rotor lamination thickness equivalent to 10% of the stator tooth width.

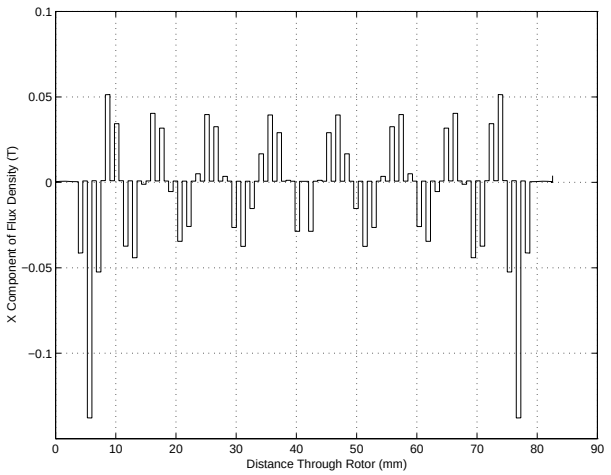

Figure 3: X Component of Magnetic Flux Density along q-axis

There are two ways in which the effect can be seen; by observation of the flux in the rotor body and an increase in the amount of q-axis flux in the return path through the stator yoke (back iron). To observe the effect in the rotor, first create an imaginary path through the rotor body, along the same path one would expect the q-axis flux to travel. If one was to observe the flux crossing this path from left to right (or right to left) then the zigzag flux will be seen. This is best described as the x-component of the flux density vectors of the FE elements that lie along this imaginary path. The graph of Figure 3 illustrates the x-component of the flux density vectors as the rotor is traversed from top (0 mm) to bottom (82.55 mm) along the physical q-axis.
The existence of zigzag flux is not just supported by Figure 3. Further confirmation is found by measuring the level of q-axis flux in the back iron of the stator. This is the main return path for q-axis flux. With the $\frac{1}{4}$ slot misalignment, the q-axis flux increases by approximately 12.5%. This is marginally less than that predicted by the analytical model developed in this paper.

4 MODELLING LEAKAGE AND AIRGAP FLUX

In addition to the q-axis modelling presented in section 2, further analysis has been performed to study the distribution of flux in the yoke and the stator teeth of the motor based on the q-axis modelling. The former provides a technique for confirming the total flux produced in the motor. Since the yoke provides the return path for the main axes flux, by finding an expression for this flux an easy comparison can be made with the FE simulation results. Consider Figure 4, which is a close up view of a small section of the motor.

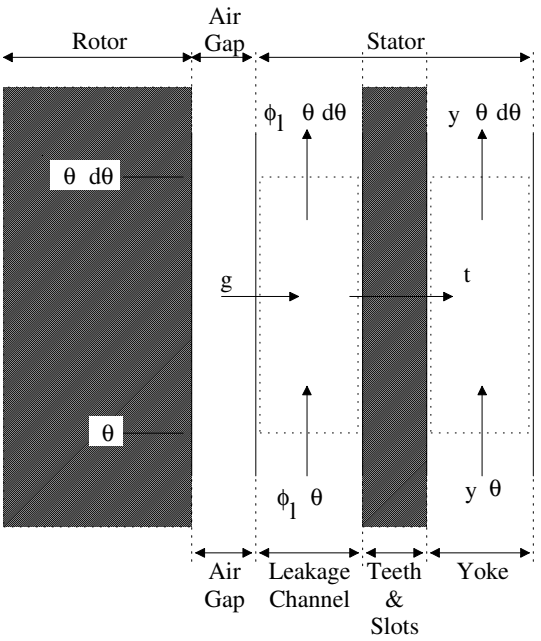

Figure 4: Stator Fluxes

As the flux in Figure 4 traverses from left to right, passage is made from the rotor through

the airgap, through the stator teeth and into the stator yoke. The airgap takes flux directly across it from the rotor with no mmf drop in the rotor. In between the airgap and the stator teeth we have defined a slot leakage channel which passes leakage flux in the direction shown. This channel runs around the circumference of the motor and the return path for leakage is through the stator yoke. An mmf drop is experienced by the leakage channel flux as it traverses the circumference of the motor. The teeth allow flux to pass from the leakage channel into the yoke with no mmf drop. Once the flux reaches the yoke it completes the closed loop path for the q-axis flux. The leakage channel has a reluctance defined as $\Re_l$ A/Wb/m of airgap. The expressions that are found for the teeth and yoke fluxes are based on the expressions for airgap flux. The value for $\Re_l$ can be found easily by utilising the known slot geometries. The expressions for the reluctance and the fluxes are given in the Appendices B and C respectively.
It should be noted that Figure 4 is a microscopic model; it only looks at the incremental angle, $d\theta$. This enables the model to be defined by a set of simple differential equations. The compromise made for this simplification is that prediction of the slotting effects cannot be made, except in as much as they have been taken into account in calculating the q-axis reluctance by using Carter's coefficient.

5 MODEL OF THE MACHINE

Several assumptions have been made in order to complete the model:

1. The teeth and slots of the stator are "smeared" into a single entity. The result of this assumption is that the slot effects on the flux distributions are neglected. This was explained previously.

2. The permeability of the iron is infinite and eddy current effects are neglected.

3. In the case of sinusoidal stator excitation, a sinusoidally distributed winding is assumed.

The method of analysis chosen requires that an expression be found for the q-axis flux in the first instance. In Figure 5 the q-axis flux is represented by the quantity Φ_q and the d-axis flux by Φ_d. The expression for Φ_q is found by considering three closed loops, as indicated by the symbols ①, ② and ③. The fine laminations of the rotor are omitted for clarity.
The circuits indicated by ① and ③ represent closed mmf circuits, whilst ② encloses a volume in which flux continuity must be maintained. The circuit ① and volume ② are intended to include only an incremental angle $d\theta$. From these fundamental circuits, the general solution for $\Phi_q(\theta)$ can be determined and is given by (1) (refer to Appendix C for further details)

$$\frac{d^2\Phi_q(\theta)}{d\theta^2} - \frac{2\mu_o R^2 L_R \Re_q}{g_e}\Phi_q(\theta) + \frac{\mu_o R^2 L_R}{g_e}\left[J(\theta) - J(\pi-\theta)\right] = 0. \tag{1}$$

In this equation, R represents the inner radius of the stator, L_R the axial length of the rotor, $\Re_q$ the q-channel reluctance and g_e is the effective air gap, which incorporates the Carter's coefficient. The angle, θ is the pole arc angle, which ranges from $\frac{-\theta_p}{2}$ to $\frac{\theta_p}{2}$, where θ_p is the pole pitch. Taking the analysis further requires knowledge of the distribution of

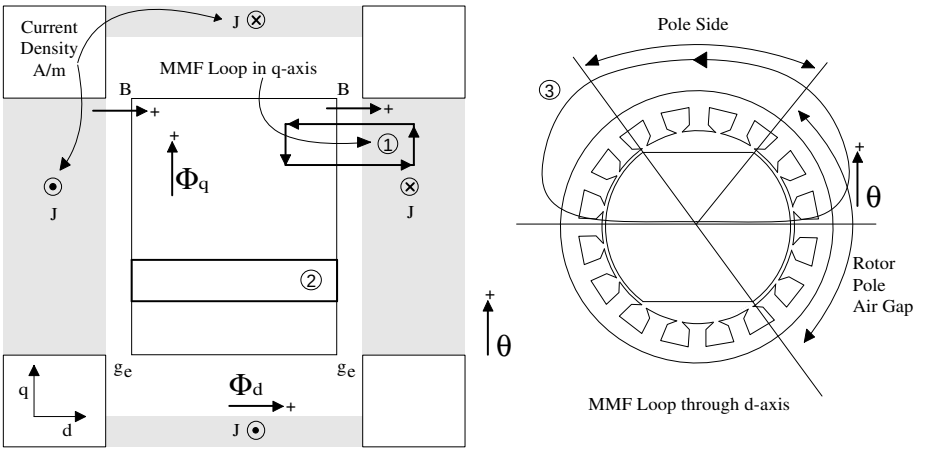

Figure 5: Machine Model

current (mmf) in the stator. In this paper, we will consider the cases where the current is sinusoidally and rectangularly distributed.
The results obtained using the analytical modelling cannot be directly compared with the results that are obtained experimentally. When results are obtained from an actual motor, all the stray effects the motor experiences are included; in particular, the end effects (end of the stator and rotor). The model presented here and the FE model both omit these end effects and it is therefore more meaningful to compare them with each other rather than with the results from a physical motor.

5.1 Pole Side Reluctance

The pole side reluctance represents the large airgap present in the q-axis flux path. Its effect is more prevalent in 2 pole motors, but essentially it has the result of drawing flux past the pole ends of the motor. The effect is due to physical constraints in the manufacture of axially laminated rotors. The width of the rotor laminations toward the end of the pole face cannot be made too small because their mechanical strength is lost. As a consequence, there is usually a larger airgap where the rotor meets the stator in the q-axis path. Figure 6 illustrates this effect.

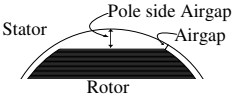

Figure 6: Pole Side Reluctance

The pole side airgap referred to in Figure 6 is not of constant length. In the analysis used in this paper, the airgap value used was an average value. That is, the expression for the pole side reluctance is based on equation (7), with the gap value set to the average value for the pole side airgap. This reluctance is referred to as $\Re_{side}$ in the equations of this paper.

5.2 Sinusoidal Current Distribution

A standard motor will have a three phase distributed winding which can be approximated by a sinusoidal distribution of current. This distribution can then be reduced into d and q-axis components. Sinusoidal current distribution is described by

$$J(\theta) = J_q \cos\theta - J_d \sin\theta. \tag{2}$$

When equation (2) is substituted into equation (1) a solution can be found for $\Phi_q(\theta)$. The solution is given as

$$\Phi_q(\theta) = J_q \left[A\left(e^{\gamma\theta} + e^{-\gamma\theta}\right) - \frac{b\cos\theta}{\Re_q(b-1)} \right]. \tag{3}$$

In this equation, the constants A, b and γ are defined in Appendix C. It is assumed that the distribution of flux is symmetric around the perimeter of the airgap; that is $B(\theta) = -B(\pi - \theta)$. The constant A is determined one of two ways; either by assuming the flux is wholly contained within the pole arc, or, some of the flux is allowed to cross the pole side. The second method is a more realistic scenario. If the latter case is to be investigated, another mmf loop is required to calculate the correct parameters. This mmf loop passes through the entire q-axis of the motor in much the same way as the d-axis mmf loop in Figure 5. Graphical representation of $\Phi_q(\theta)$ is given in Figure 7.

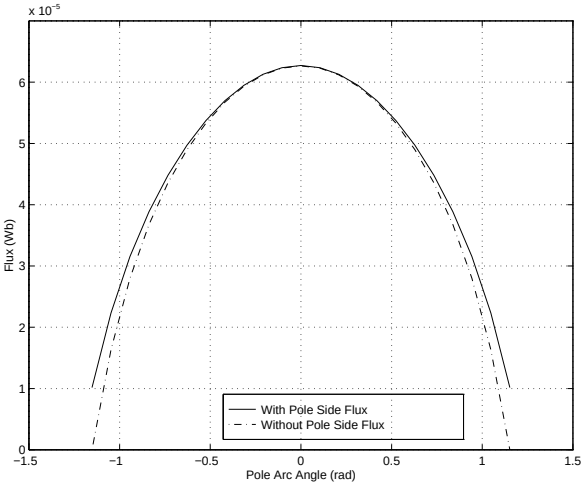

Figure 7: Flux vs Pole Arc Angle, Sinusoidal Current Distribution

Once an expression has been found for the q-axis flux, it is possible to derive a relationship for the airgap flux density distribution. The solution turns out to be

$$B(\theta) = -\frac{1}{2}\left[\frac{J_q}{RL_R}\left[\gamma A\left(e^{\gamma\theta} + e^{-\gamma\theta}\right) + \frac{b\sin\theta}{\Re_q(b-1)} \right] - \frac{2\mu_o R J_d \cos\theta}{g_e} \right]. \tag{4}$$

A graphical representation of this expression is illustrated in Figure 8.

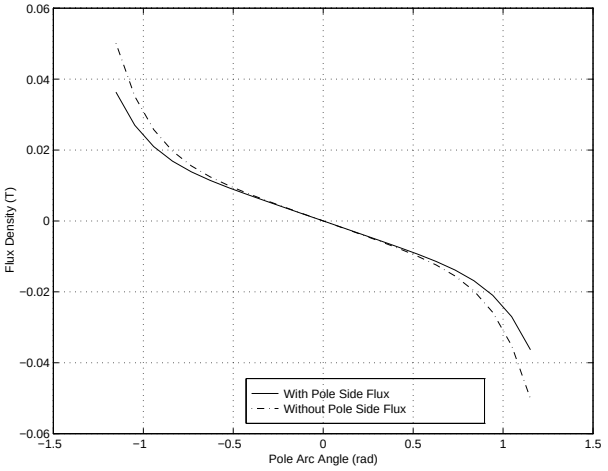

Figure 8: Airgap Flux Density vs Arc Pole Angle, Sinusoidal Current

The best place to observe the total flux in the motor is in the the yoke or back iron of the machine. Whatever q-axis flux there is, it must form a complete circuit via the yoke. Three results are obtained; the total flux in the yoke from the FE simulation with an aligned and misaligned rotor, and results from the analytical modelling.

Total Flux, FE Analysis, aligned rotor	22.4 μWb
Total Flux, FE Analysis, misaligned rotor	25.2 μWb
Total Flux, Modelling	25.8 μWb

This is an acceptable result. The two values to compare are those of the FE analysis using the misaligned rotor and the modelling values. The modelling has the effect of the misaligned rotor included. These values compare favourably which leads us to the conclusion that the analytical model provides a reasonable insight into the flux level of the SRM.

5.3 Rectangular Wave Current Distribution

The synchronous reluctance motor is a motor which operates with the greatest possible fluxing if the poles carry uniform flux across their faces. This leads to a flux waveform in the airgap which would be quasi-square. Under these conditions, the motor will produce maximum torque per watt of copper loss if the q-axis current is in the form of square blocks, located opposite the pole faces. Similarly, the most efficient way of distributing the magnetising current is in a square block at the side of the pole. In practice, this situation could be approximated with a large number of phases, each phase consisting of a single, fully pitched coil. It can be represented in the model as a quasi-square current distribution, the two levels being set by the required mmf along each axis.
Mathematically, we need only to express the function for the current density as J rather than $J(\theta)$. Due to symmetry, J at $(\pi-\theta)$ is the same as $-J$ at (θ). The solution to equation (1) for the rectangular current case becomes

$$\Phi_q(\theta) = J_q \left[A \left(e^{\gamma\theta} + e^{-\gamma\theta} \right) - \frac{1}{\Re_q} \right]. \tag{5}$$

There are two scenarios to consider; with and without pole side flux. Both situations lead to the same solution for $\Phi_q(\theta)$, but the constant A is different. Figure 9 is a graphical representation of $\Phi_q(\theta)$.

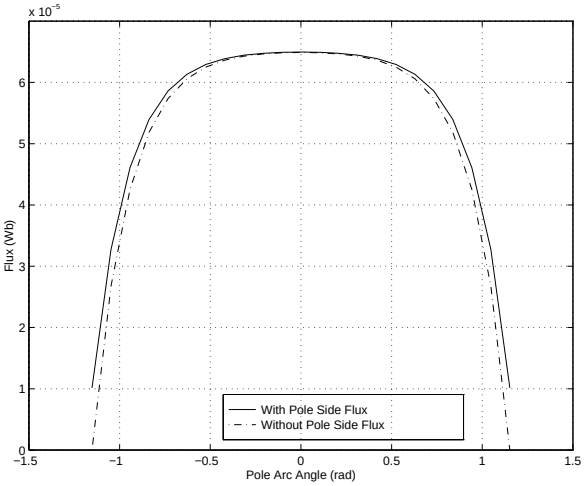

Figure 9: Flux vs Pole Arc Angle, Rectangular Current Distribution

The airgap flux density for the q-axis is partially derived in Appendix C and the main result is

$$B(\theta) = -\frac{1}{2} \left[\frac{J_q \gamma A}{R L_R} \left(e^{\gamma\theta} - e^{-\gamma\theta} \right) - \frac{\mu_o R J_d \left(\pi - \theta_p \right)}{g_e} \right]. \tag{6}$$

A graphical representation of this expression is given in Figure 10.

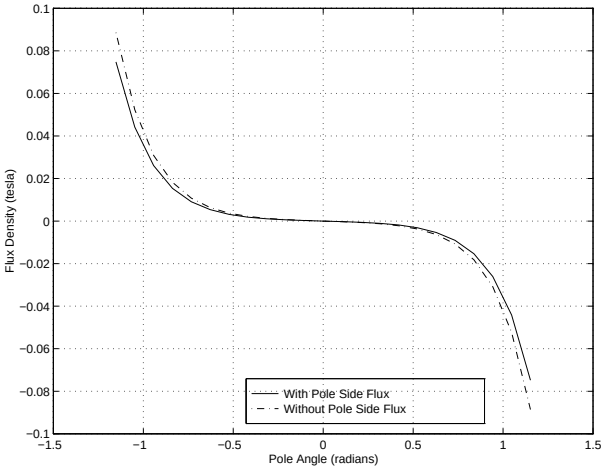

Figure 10: Airgap Flux Density vs Pole Arc Angle, Block Current

The total flux in the motor is a quantity that is more likely to yield results similar to the FE analysis. The modelling does not predict the level of zigzag flux that occurs, but rather the overall effect on the fluxing of the motor. The modelling and simulations produce the following results, where the agreement is very good.

Total Flux, FE Analysis, aligned rotor	23.92 μWb
Total Flux, FE Analysis, misaligned rotor	26.73 μWb
Total Flux, Modelling	26.96 μWb

6 COMMENTS AND CONCLUSIONS

The greatest difficulty with previous analytical models was the inadequacy of the q-axis modelling. One of the reasons why this modelling was incomplete was the the omission of the zigzag effect that has been introduced in this paper. In [8] much work was performed in determining the optimum number of laminations required in an axially laminated rotor in order to maximise the saliency ratio. However, whilst increasing the number of laminations has the desired effect of reducing torque ripple, if the number is increased such that the thickness of the rotor lamination is of the order of 10% of the stator tooth, then the saliency ratio will be reduced as a direct result of these zigzag flux paths. This has a further negative impact upon calculations involving efficiency and power factor for example.
The results from the work presented in this paper indicate that there is a point beyond which the gains made by using thinner laminations are diminished and in fact a reduction in saliency will occur. There should be an optimal value for the thickness of the lamination. The introduction of an expression for the q-channel reluctance is important since it relates the physical dimensions of the synchronous reluctance motor to the q-axis inductance. The calculation of the q-channel reluctance enables the development of expressions for the flux distribution in the airgap of the motor. Whilst these expressions do not predict the variations in airgap flux due to zigzag effects, they do include the average effect on the overall fluxing of the motor. The flux densities predicted by this model are comparable with the values predicted by a finite element analysis. Overall, this paper represents a significant

improvement in the modelling of the q-axis of the SRM by introducing concepts that have been neglected in previous research.

A MOTOR PARAMETERS

Voltage	440 V	Current	3.3 A
Rotor Radius	41.15mm	Stator (inner) Radius	41.3mm
Stator Length	46.1mm	Rotor Length	44.8mm
No. Stator Slots	24	Pole Pairs	1
Air Gap	0.25mm	K_a	0.5

Table 1: SRM Physical Parameters

The quantity K_a is the ratio of the thicknesses of magnetic to non-magnetic material in the rotor. The Stator Radius is defined as the inner radius.

B RELUCTANCE EQUATIONS

B.1 Q-Channel Reluctance

A general expression for reluctance is given by

$$\Re = \frac{l}{\mu_o A}. \tag{7}$$

In equation (7), l represents length, A the surface area and μ_o the permeability constant, $4\pi * 10^{-7}$A/m. This general expression is used as the basis for all reluctance calculations in the modelling. First consider the airgap reluctance expressions (refer to G1 and G2 in Figure 2(b). The area term, A of the above expression is determined from the surface area of the tooth face A_s. In the case of airgap $G1$, this is represented by $0.25A_s$ and in the case of airgap $G2$ by $0.75A_s$. The airgap length for both $G1$ and $G2$ are the same. Therefore the expressions for these two air gap reluctances is

$$\Re_{G1} = \frac{g_e}{0.25\mu_o A_s}, \quad \Re_{G2} = \frac{g_e}{0.75\mu_o A_s}. \tag{8}$$

In these expressions, the quantity g_e represents the effective airgap length. The simple physical airgap length cannot be used since both the rotor and the stator are slotted. This slotting effect can be taken into account by the use of Carter's coefficient. The effective airgap length is given by the expression

$$g_e = gK_{c1}K_{c2}, \tag{9}$$

where K_{c1} is the Carter's coefficient due to the stator slotting and K_{c2} is the Carter's coefficient due to the alternate layers of magnetic and non-magnetic material in the rotor and g the actual airgap. Finally, the expression for the reluctance through the rotor body itself is to be determined. These are the reluctances represented by the terms B, C & D in Figure

2(b). There is a slight complication in finding the expression for these values; the rotor is cylindrical. A consequence of this is that the value of A, the cross-sectional area, changes as the rotor body is traversed. In this analysis, we use an integral average value. Thus, the expression for this reluctance is given by

$$\Re_R = \frac{0.5 l_{sp}}{\mu_o A_{rl}} K_a, \tag{10}$$

where l_{sp} is the length of the slot pitch (one tooth plus one slot), A_{rl} is the average surface area of the cross section of the rotor and K_a is a constant expressing the ratio between magnetic and non-magnetic material in the rotor.
With these expressions, there is a method of determining the q-channel reluctance from the motor parameters. The analysis treats the problem as a network of resistors in which the resistive elements are like those present in Figure 2(b). The final value of reluctance which has the unit of A/Wb is normalised to an A/Wb/m value by multiplying the result by $1000/l_{sp}$ (l_{sp} is given in millimetres). This final step is only required for further analysis as presented in this paper.

B.2 Slot Leakage Reluctance

Finding an expression for the slot leakage reluctance first requires definition of the physical system that is being modelled. Figure 11 illustrates the basis of the modelling for this parameter.

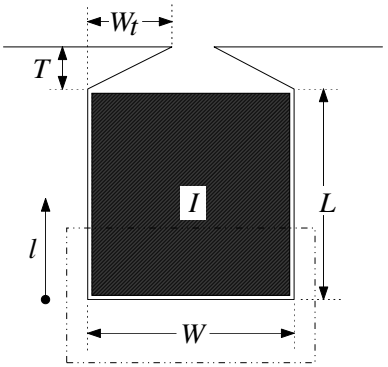

Figure 11: Slot Leakage Reluctance Model

The physical quantities are self explanatory, being dimensions of the tooth slot. The quantity l is used to express the incremental distance traversed from the base of the slot towards the top of the slot, but less than the height L. The block marked I represents the current density in the slot of the motor. The expression for leakage reluctance is found by first determining an expression for the reluctance of the area enclosed in the section bounded by W and L. Next, a similar expression is found for the upper area of the slot; the trapezoidal shaped section. The complete expression is these two reluctances arranged in a parallel circuit. The first section of interest is the rectangular section bounded by W and L in Figure 11. In this section, the currently is uniformly distributed in the slot such that

$$J = \frac{I}{WL}. \tag{11}$$

The total mmf enclosed by the closed loop is

$$MMF = JWl. \tag{12}$$

This value for enclosed mmf must be equal to the mmf dropped by flux crossing the slot

$$MMF = HW. \tag{13}$$

where H is the magnetic field intensity. By equating this expression with the well known relationship $B = \mu_o H$ and substituting equation (12), we obtain

$$B = \frac{\mu_o Il}{WL}. \tag{14}$$

Now, the total flux enclosed in the slot is

$$\phi = \int_0^L BL_s\, dl. \tag{15}$$

where L_s represents the length of the stator stack. Solution of this integral leads to

$$\phi = \frac{\mu_o IL_s L}{2W}. \tag{16}$$

Since reluctance is defined by flux and magnetomotive force, an expression for reluctance is found by substitution and leads to

$$\Re_{l1} = \frac{2W}{\mu_o L_s L}. \tag{17}$$

To include the effects of the trapezoidal opening of the slot, consider the mmf in this area given by

$$MMF = H\left(W - \frac{2lW_t}{T}\right). \tag{18}$$

Once again an expression for B is found by substituting equation (18) into $B = \mu_o H$ and simplifying to get

$$B = \frac{\mu_o IT}{WT - 2lW_t}. \tag{19}$$

The total flux enclosed by the tooth tip uses equation (15) except that l traverses the region indicated by parameter T

$$\phi = \int_0^T BL_s\, dl. \tag{20}$$

Solution of this integral leads to an expression for the flux in the tooth tip area

$$\phi = \frac{\mu_o I T L_s}{2W_t}\left[\ln\left(1 - \frac{2W_t}{W}\right)\right]. \tag{21}$$

Finally, the expression for reluctance in this area can be expressed as

$$\Re_{l2} = \frac{-2W_t}{\mu_o L_s T\left[\ln\left(1 - \frac{2W_T}{W}\right)\right]}. \tag{22}$$

Equation (22) is an expression for the reluctance of one slot/tooth pair in the stator. When combined with equation (17) as a parallel circuit, the complete expression for slot leakage reluctance as used in this analysis is found.

C FLUX EQUATIONS

C.1 General Solution for Q-Axis Flux

The analysis for the q-axis flux general solution is based on Figure 5, following the path around loop ① in the direction shown, leads to the expression

$$J(\theta)R d\theta = \Phi_q(\theta)R\Re_q - \frac{g_e}{\mu_o}\frac{dB(\theta)}{d\theta}. \tag{23}$$

The expression for continuity of flux enclosed by region ② leads to the expression

$$\frac{d\Phi_q(\theta)}{d\theta} - RL_R\left[B(\pi-\theta) + B(\theta)\right] = 0. \tag{24}$$

Finally, the mmf loop ③ through the d-axis produces

$$\int_\theta^{\pi-\theta} J(\theta)R\, d\theta = \frac{g_e}{\mu_o}\left[B(\theta) - B(\pi-\theta)\right]. \tag{25}$$

The above three equations are manipulated to produce a simple differential equation for the q-axis flux as a function of pole arc angle θ. This differential equation for $\Phi_q(\theta)$ turns out to be

$$\frac{d^2\Phi_q(\theta)}{d\theta^2} - \frac{2\mu_o R^2 L_R \Re_q}{g_e}\Phi_q(\theta) + \frac{\mu_o R^2 L_R}{g_e}\left[J(\theta) - J(\pi-\theta)\right] = 0. \tag{26}$$

From this equation, some simple constants are defined. These are;

$$b = \frac{2\mu_o R^2 L_R \Re_q}{g_e}, \quad C = \frac{b}{2\Re_q}. \tag{27}$$

Now, equation (26) can be re-written as

$$\frac{d^2\Phi_q(\theta)}{d\theta^2} - b\Phi_q(\theta) + C\left[J(\theta) + J(\pi - \theta)\right] = 0. \tag{28}$$

The solution to equation (28) is an expression that represents the equation for the q-axis flux. This solution is dependent upon the function adopted for the current density, J.

C.2 General Solution for Yoke Flux

In this section, we will investigate the general solution for the yoke flux distribution. There are two ways to determine the q-axis flux that should appear in the yoke of the motor; by direct analysis or by calculation knowing the geometry of the motor and the expression for the q-axis flux previously derived. Both methods should lead to the same result. Figure 4 gives the model used for this analysis. If the stator current is expressed as $J(\theta)$ amperes per metre, then we can write

$$\phi_l = \frac{J(\theta)}{\Re_l}. \tag{29}$$

Next, consider the continuity of flux in the region defined as the slot leakage channel

$$B_g(\theta) R d\theta L_s - B_t(\theta) R d\theta L_s + \phi_l(\theta) - \phi_l(\theta + d\theta). \tag{30}$$

The quantity L_s represents the axial length of the stator. The collection of like terms and further simplification leads to a more useful expression

$$\frac{d\phi_l(\theta)}{d\theta} = RL_s\left(B_g - B_t\right). \tag{31}$$

Now consider the continuity of flux in the region located within the yoke of the motor

$$B_t(\theta) R d\theta L_s - B_y(\theta) Y L_s - B_y(\theta + d\theta) Y L_s = 0. \tag{32}$$

Simplification of this equation also leads to a more useful expression

$$\frac{dB_y(\theta)}{d\theta} = \frac{R}{Y} B_t(\theta). \tag{33}$$

Equations (29), (31) and (33) are general solutions and can be used in combination to solve for the equations that describe yoke and stator tooth flux density.

C.3 Sinusoidal Current Distribution

The solution to equation (28) for the sinusoidal current distribution case is given by the following expression

$$\Phi_q(\theta) = J_q \left[A \left(e^{\gamma\theta} + e^{-\gamma\theta} \right) - \frac{b\cos\theta}{\Re_q(b-1)} \right]. \tag{34}$$

If the case of no pole side flux was being considered, A would be defined as

$$A = \frac{b\cos\frac{\theta_p}{2}}{\Re_q(b-1)\left(e^{\gamma\frac{\theta_p}{2}} + e^{-\gamma\frac{\theta_p}{2}} \right)}. \tag{35}$$

If the case of pole side flux was being considered, A would be defined as

$$A = \frac{\gamma}{\Re_q(b-1)} \frac{\Re_q R(b-1) + b\left[\Re_q R\sin\frac{\theta_p}{2} + \Re_{side}\cos\frac{\theta_p}{2} \right]}{\Re_q R\left(e^{\gamma\frac{\theta_p}{2}} - e^{-\gamma\frac{\theta_p}{2}} \right) + \gamma\Re_{side}\left(e^{\gamma\frac{\theta_p}{2}} - e^{-\gamma\frac{\theta_p}{2}} \right)}. \tag{36}$$

Equation (34) is the expression that describes the q-axis flux of the motor for the case of sinusoidally distributed stator currents. Also,

$$\gamma = \sqrt{b}. \tag{37}$$

If we substitute the expression for the current distribution, equation (2), into equation (25) and perform the required integration then substitute this result into equation (24), a solution for the airgap flux densities is obtained

$$B(\theta) = -\frac{1}{2}\left[\frac{J_q}{RL_R}\left[\gamma A\left(e^{\gamma\theta} + e^{-\gamma\theta} \right) + \frac{b\sin\theta}{\Re_q(b-1)} \right] - \frac{2\mu_o R J_d\cos\theta}{g_e} \right]. \tag{38}$$

Once this result is obtained, we can derive an expression for the q-axis yoke flux

$$\begin{aligned} B_{yq}(\theta) = -\frac{J_q}{2YL}\Bigg[& A\left(e^{\gamma\theta} + e^{-\gamma\theta} \right) - \frac{b\cos\theta}{\Re_q(b-1)} - \frac{\cos\theta}{\Re_l} \\ & -A\left(e^{\gamma\frac{\theta_p}{2}} + e^{-\gamma\frac{\theta_p}{2}} \right) + \frac{b\cos\frac{\theta_p}{2}}{\Re_q(b-1)} + \frac{\cos\frac{\theta_p}{2}}{\Re_l} \Bigg]. \end{aligned} \tag{39}$$

C.4 Rectangular Wave Distribution

The solution for the block current distribution is given by the expression

$$\Phi_q(\theta) = J_q \left[A \left(e^{\gamma\theta} + e^{-\gamma\theta} \right) - \frac{1}{\Re_q} \right]. \tag{40}$$

If the case of no pole side flux was being considered, A would be defined as

$$A = \frac{1}{\Re_q \left(e^{\gamma \frac{\theta_p}{2}} + e^{-\gamma \frac{\theta_p}{2}} \right)}. \tag{41}$$

If the case of pole side flux was being considered, A would be defined as

$$A = \frac{\gamma}{\Re_q} \frac{\Re_q R \theta_p + \Re_{side}}{\Re_q R \left(e^{\gamma \frac{\theta_p}{2}} - e^{-\gamma \frac{\theta_p}{2}} \right) + \gamma \Re_{side} \left(e^{\gamma \frac{\theta_p}{2}} + e^{-\gamma \frac{\theta_p}{2}} \right)}. \tag{42}$$

Using the same substitutions to that for the sinusoidal case, an expression for the airgap flux densities is also derived

$$B(\theta) = -\frac{1}{2} \left[\frac{J_q \gamma A}{R L_R} \left(e^{\gamma \theta} - e^{-\gamma \theta} \right) - \frac{\mu_o R J_d \left(\pi - \theta_p \right)}{g_e} \right]. \tag{43}$$

From this point, using previously derived relationships for airgap and stator tooth fluxes, an expression can be found for the q-axis yoke flux

$$B_{yq}(\theta) = \frac{-J_q A \left(e^{\gamma \theta} - e^{-\gamma \theta} - e^{\gamma \frac{\theta_p}{2}} - e^{-\gamma \frac{\theta_p}{2}} \right)}{2 Y L_R}. \tag{44}$$

REFERENCES

[1] I. Marongiu and A. Vagati, "Improved Modelling of a Distributed Anisotropy Synchronous Reluctance Machine", in *Proceedings of the IEEE Industry Applications Society Annual Meeting*, 1991, pp. 238–243.

[2] I. Boldea, Z. X. Fu, and S. A. Nasar, "Performance Evaluation of Axially-Laminated Anisotropic (ALA) Rotor Reluctance Synchronous Motors", *IEEE Transaction on Industry Applications*, Vol. 30, No. 4, pp. 533–554, July/August 1994.

[3] X. Luo, A. El-Antably, and T. A. Lipo, "Multiple Coupled Circuit Modeling of Synchronous Reluctance Machines", in *Proceedings of the IEEE Industry Applications Society Annual Meeting*, 1994, Vol. 1, pp. 281–289.

[4] A. Fratta, G. P. Troglia, A. Vagati, and F. Villata, "Evaluation of Torque Ripple in High Performance Synchronous Reluctance Machines", in *Proceedings of the IEEE Industry Applications Society Annual Meeting*, 1993, Vol. 1, pp. 163–170.

[5] P. P. Ciufo, D. Platt, and B. S. P. Perera, "Magnetic Circuit Modelling of a Synchronous Reluctance Motor", in *Proceedings of the Australian Universities Power Engineering Conference*, 1994, pp. 37–42.

[6] D. A. Staton, W. L. Soong, and T. J. E. Miller, "Unified Theory of Torque Production in Switched Reluctance and Synchronous Reluctance Motors", *IEEE Transactions on Industry Applications*, Vol. 31, No. 2, pp. 329–336, March/April 1995.

[7] K. Uezato, T. Senjyu, and Y. Tomori, "Modelling and Vector Control of Synchronous Reluctance Motors Including Stator Iron Loss", *IEEE Transactions on Industry Applications*, Vol. 30, No. 4, pp. 971–976, July/August 1994.

[8] D. A. Staton, T. J. E. Miller, and S. E. Wood, "Maximising the Saliency Ratio of the Synchronous Reluctance Motor", *IEE Proceedings Part B*, Vol. 140, No. 4, pp. 249–259, July 1993.

[9] T. Matsuo and T. A. Lipo, "Rotor Design Optimisation of Synchronous Reluctance Machine", *Transactions on Energy Conversion*, Vol. 9, No. 2, pp. 359–365, June 1994.

[10] D. Platt, "Reluctance Motor with Strong Rotor Anisotropy", *IEEE Transactions on Industry Applications*, Vol. 28, No. 3, pp. 652–658, May/June 1992.

[11] J. E. Fletcher, T. C. Green, and B. W. Williams, "Vector Control of a Synchronous Reluctance Motor Utilising an Axially Laminated Rotor", in *IEE Conference Proceedings Power Electronics and Variable-Speed Drives*, 1994, pp. 18–23.

[12] J. D. Law, A. Chertok, and T. A. Lipo, "Design and Performance of Field Regulated Reluctance Machine", *IEEE Transactions on Industry Applications*, Vol. 30, No. 5, pp. 1185–1191, September/October 1994.